Correlating droplet size with temperature changes in electrospray source by optical methods.

Antonin Soleilhac, Xavier Dagany, Philippe Dugourd, Marion Girod,
Rodolphe Antoine

Correlating droplet size with temperature changes in electrospray source by optical methods.

Antonin Soleilhac,[a] Xavier Dagany,[a] Philippe Dugourd,[a] Marion Girod[b] and Rodolphe Antoine[a],*

[a]Institut lumière matière, UMR5306 Université Claude Bernard Lyon1-CNRS, Université de Lyon 69622 Villeurbanne cedex, France.

[b]Institut des Sciences Analytiques, UMR 5280 CNRS Université Lyon1, Université de Lyon 69622 Villeurbanne cedex, France.

ABSTRACT: We investigated how the temperature and size of charged droplets are affected by the electrospray ionization (ESI) process, using *in situ* measurements involving laser-induced fluorescence and Mie scattering on a thermal gradient focusing ESI source. Rhodamine dyes were employed as temperature indicators using ratiometric intensity based fluorescence techniques. The results were compared to lifetime-based techniques using tris(2,2'-bipyridyl)dichlororuthenium(II) hexahydrate, $[Ru(bpy)_3]^{2+}$). Both methods gave similar profiles. Nevertheless, the precision and sensitivity were higher for lifetime-based techniques in comparison to intensity-based techniques. Global warming (with $\Delta T \sim 10$ K) of the ESI plume is reported while the size of the droplet decreases along the plume. The global warming indicates that the conductive thermal transfer (between the super-heated sheath gas and the solvent) is predominant and stronger than the cooling effect due to the evaporation of the droplets, and is well reproduced by a diffusion-controlled evaporation model. Thermal gradient focusing ESI sources therefore appear efficient sources for evaporating large amounts of solvent, along with an increase in temperature.

Making improvements in sensitivity and efficiency for electrospray ionization (ESI) has been a challenge over the past few decades. These improvements are important for multiple analytical applications. Since the pioneering work of Fenn et al. in the 1980s,[1, 2] the ESI source has continued to undergo various changes in its size, material, and geometry.[3] These transformations were performed to optimize both ionization efficiency and the efficiency of transferring ions from the solution to the gas phase in the mass analyzer. High-flow electrospray sources (>5-10 μL/min) are normally combined with a supply of heat within the source housing to facilitate the evaporation of solvents. The evaporation of large amounts of solvent is important for evaporation to occur at the optimum position within the ESI plume to ensure maximum transmission and the reduction of ion solvent clusters in high flow electrospray source designs. The use of a drying gas and a heated capillary can influence the system's robustness and reduce the degree of cluster ion formation.[4]

The transfer of analyte ions from solution to gas phase is not an exoenergetic process, as the desolvation process cools the droplets and then the gaseous ions without heat supply. Consequently, the temperature changes within the spray plume are of utmost importance and may have dramatic consequences for kinetically labile equilibrium reactions[5, 6] and for conformational changes in proteins[7, 8] studied by electrospray ionization mass spectrometry. Following the electrical atomization of the liquid to form the droplets in the ESI source, the droplet temperature is thermalized to the ambient bath gas temperature, minus the small cooling effect due to solvent evaporation. Kebarle assumed that droplets in an ESI source behave like neutral droplets evaporating in air in the absence of an electric field and estimated that the decrease of droplet temperature could be in the range of 10 K.[9] Recently, the evolution of droplet temperatures in an electrospray plume was measured using ratiometric fluorescence.[10] Under typical operating conditions, droplet temperatures decrease by ∼30 K over the first 5.0 mm along the spray axis, followed by a slight (∼2–3 K) rewarming, but to our knowledge there have been no experimental determinations of both temperatures and droplet sizes, which limits the quantitative description of mass and heat transfer in an ESI plume. This description can be further complicated when super-heated sheath gases are used, in particular with thermal gradient focusing ESI sources, where cooling may be countered by heated background gas.
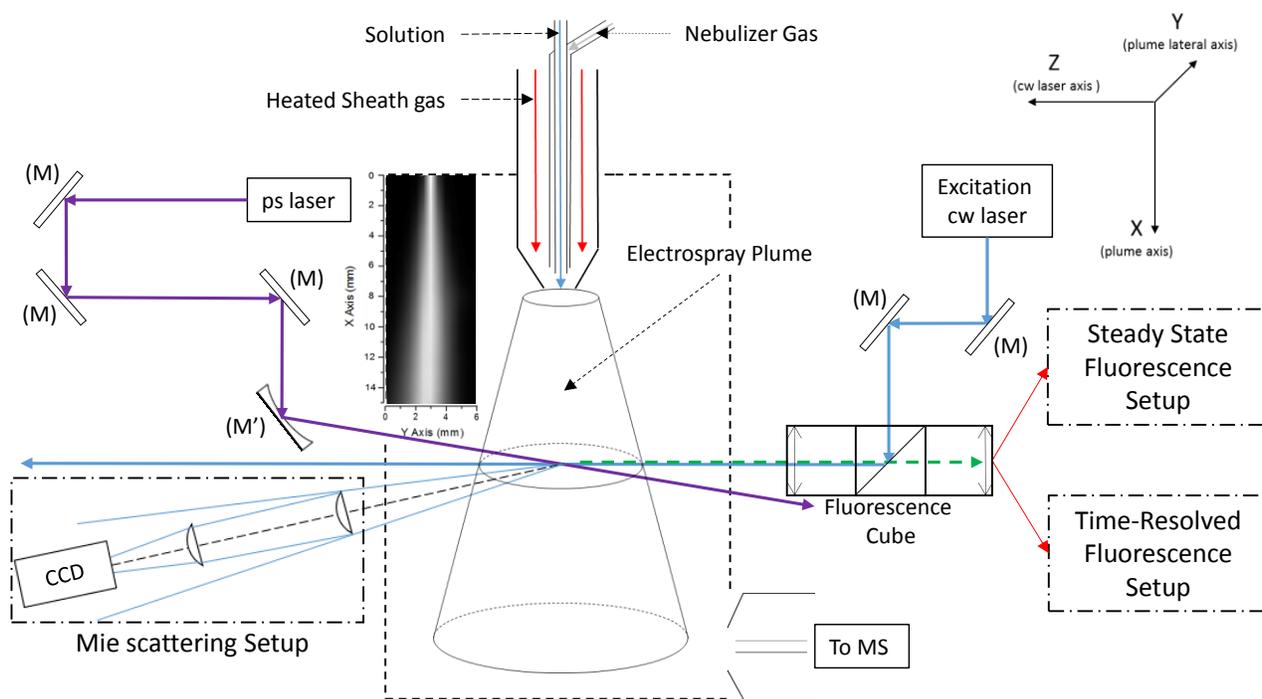
Figure 1: Schematic diagram of the experimental setup used to probe the temperature and the droplet size in the Agilent jet Stream plume. Inset: profile of the ESI plume recorded by plotting the maximal intensity (White ~104 counts – Black ~100 counts) of the fluorescence spectrum of a solution of Rhodamine 110 at 20 μM in methanol. The position of the electrospray nozzle exit is X=0 mm and Y=3 mm and the MS capillary inlet is X=15 mm and Y≃8 mm.

Techniques for probing the evolution of charged droplet size, temperature, and composition are essential to fully characterize mass and heat transfer mechanisms.[11, 12] The evolving size, composition, and temperature of evaporating ethanol/water aerosol droplets 25−57 μm in radius were probed by cavity enhanced Raman scattering (CERS) and laser induced fluorescence.[12] Concerning ESI sources, in the pioneering work by Zhou and Cook,[13-15] the change in solvent composition in solvent mixtures was studied along the electrospray plume, using a solvatochromic dye and laser-induced fluorescence (LIF) measurements. The same strategy was used by Wang and Zenobi[16] to probe the evolution of solvent polarity along the electrospray plume. We recently proposed a new experimental approach that combines *in situ* measurements by optical methods with mass spectrometry measurements.[17] In particular, this coupling allowed us to measure simultaneously mass spectra and pH profiles to study the relation between the charge states of peptide and protein anions in mass spectra and pH changes in the spray plume.[17-19]

Based on the current state-of-the-art of spray imaging, we propose a new experimental approach that combines *in situ* laser-induced fluorescence and Mie scattering measurements, which allows us to probe changes in temperature and droplet size along the ESI plume. A ratio- metric evaluation of fluorescence intensity using dyes[20, 21] has been proposed to determine temperature, but it is often affected by dye concentration, excitation efficiency and detection efficiency.[21] As an alternative to these intensity-based methods, lifetime-based methods, in principle, can provide a more robust measure of temperature.[22] This is owing to the high sensitivity of the non-radiative

decay rate to temperature changes exhibited by some fluorescent species. To this end, we implemented a fluorescence lifetime- and intensity-based profiling setup in conjunction with a microdroplet sizing scheme on a modified Agilent Jet Stream electrospray[23] source coupled to a single quadrupole mass analyzer. The optical setup permits profiling the temperature and the size of the droplets as they evaporate in the electrospray plume, by measuring both the angular scattering pattern and emission spectra. In this work, two different strategies for measuring the temperature of the droplets are employed and compared: (i) lifetime of the thermochromic Tris(2,2′-bipyridyl)dichlororuthenium(II) hexahydrate complex[24] and (ii) a ratiometric, two-color LIF thermometry approach with thermochromic rhodamine B and rhodamine 110, the latter being used as an internal standard. We also correlate the temperature changes along the ESI plume with the evolution of droplet size and compare the results to evaporative models to provide insight into the mechanisms of mass and heat transfer in thermal gradient focusing ESI sources.

EXPERIMENTAL SECTION

The experimental setup for ESI plume profiling is illustrated in Figure 1. An Agilent Jet Stream electrospray source has been slightly modified to allow *in situ* laser injections coupled with three different optical detection systems mounted on a moving stage. The three different optical detection systems allow recording both steady-state and time-resolved fluorescence signals and collecting, using Mie scattering measure-

ments, the diffracted light (fringe patterns) as a function of the scattering angle. The different parts of the set-up are described in detail in the following paragraphs.

Mass spectrometer. The experiments were performed on a Single Quad 6100 equipped with the modified Agilent Jet Stream (AJS) ESI source (Agilent Technologies, Santa Clara, CA, USA). Nitrogen was used as the nebulizing gas and the drying gas. The polarity switching mode was used to obtain both positive and negative spectra. The capillary voltage was set at $C_v^+ = 2000$ V and $C_v^- = 3000$ V and the nozzle voltage at $C_n^+ = 500$ V, $C_n^- = 500$ V. Agilent Jet Stream technology utilizes super-heated nitrogen gas to desolvate the droplets and confine the electrospray plume. The temperature of the sheath gas must be between 353 K and 643 K to ensure optimal ESI source efficiency. The source cannot be used at temperatures below 353 K due to spray instabilities. The temperature of the super-heated sheath gas (SGT) is set at 373 K, 423 K or 523 K and the flow of the super-heated sheath gas (SGF) is set at 3 L/min, 7 L/min or 11 L/min according to the experiment. The nebulizer gas pressure (NGP) is set at 10 PSI, 25 PSI or 50 PSI according to the experiment. Solutions are introduced into the ionization source at a sampling flow rate of F = 3mL/h (50μL/min) with a KDS100 syringe pump (KD Scientific, Holliston, MA, USA). The Agilent ChemStation software provided by Agilent Technologies was used for instrument control, data acquisition and data processing.

Chemicals. Rhodamine 110 Chloride and Rhodamine B Chloride were purchased from lambda physik (Lambdachrome Laser Dye). Tris(2,2′-bipyridyl)dichlororuthenium(II) hexahydrate ($[Ru(bpy)_3]^{2+}$) was purchased from Sigma Aldrich (Sigma Aldrich, St Louis, MO, USA). No further purification was needed. Methanol (MeOH) from Fisher Chemical was used as solvent. Separated 1 mM stock solutions were prepared in methanol or water and then diluted according to the experiments. $[Ru(bpy)_3]^{2+}$ solutions were purged of O_2 before the fluorescence measurements according to the protocol described in the supporting information.

Optical objective & Fluorescence Cube. An Optem 125C lens (Thales Optem Inc., Fairport, NY, USA) was used for to inject the focused continuous wavelength laser beam and collect the fluorescence signals with a working distance of ~100 mm. A fluorescence cube was placed between the laser and the objective. It was composed of an excitation filter (band pass 473 ± 5 nm or 532 ± 5 nm according to the experiment) a dichroic mirror (473 nm or 532 nm) and a high pass filter (cutoff at 473 nm or 540 nm). This configuration allowed us to collect the fluorescence signal emitted on the same axis (epi-fluorescence configuration) without any "laser peak" by separating the excitation and the emission light components. The injection of the fluorescence signal into an optical fiber (diameter 600 μm) was done using a microscope lens (n.a. = 0.25, f = 2.5mm).

Steady State Fluorescence (SSF) Setup. A MBL-F-473-500 laser (Changchun New Industries Optoelectronics Technology Co., Ltd) is used for excitation. The output power of the laser is 500 mW at 473 nm and its beam diameter is 3 mm (divergence 1.5 mrad). The laser is injected through the objective using two protected, flat reflecting aluminum mirrors (R>90%). Steady-state fluorescence (SSF) spectra were recorded using an Ultra-compact spectrophotometer Econic

(B&WTek Inc., Newark, DE, USA) with a resolution of 1.5 nm via an optical fiber. The spectrophotometer was cooled to 280 K using an external oil circulator (Haake Phoenix II P1, Thermo Scientific, Karlsruhe,Germany) and a brass tank surrounding the spectrophotometer.

Two-color ratiometric Laser Induced Fluorescence thermography was used for temperature profiling in SSF configuration. Rhodamine B was used as a thermochromic dye (its fluorescence spectrum is highly sensitive to temperature), whereas Rhodamine 110 was used as a reference for ratiometry measurements. For rhodamine B, an increase in the non-radiative decay rate with increasing temperature leads to both fluorescence intensity and lifetime decreases. Lifetime of rhodamine B in methanol (at room temperature) is 1.68 ns, and time-resolved fluorescence would require picosecond time resolution for the detection scheme (not available in our lab). Fluorescence signals of a mixture of Rhodamine 110 at 0.2 μM and Rhodamine B at 2 μM in methanol were recorded in solution at different temperatures using a home-made temperature-controlled cell in an epi-fluorescence configuration. The cell was made of aluminum and comprised three quartz windows sealed by o-rings. The two on-axis windows allowed the injection and ejection of the laser. The collection of fluorescence could be performed either in an epi-fluorescence configuration or by using a third window at 90° and coupled to an optical fiber via an SMA connector. A heating finger (Thermocoax, Redring) and a PT100 thermocouple were inserted in the thermostat. This system allows accurate temperature control (from ~288 K to ~423 K) in the sample after temperature equilibration. The cell volume was about 3 mL. Calibration curves ($I_{max}^{RhB}/I_{max}^{Rh110}$ ratio as a function of temperature) were then established in MeOH solution (Fig. S1 in supporting information). For the fluorescence measurements from the electrospray plume, the exposure time for each step was set to 10 s. Typical fluorescence spectra are given in Fig. S2 in the supporting information for several points of the ESI plume axis.

Time-Resolved Fluorescence (TRF) Setup. A picosecond laser (PGx03 series Optical Parametric Generators (OPG) from EKSPLA) pumped by a 1 kHz mode-locked laser was used for excitation. The optical design is optimized to produce low divergence at a pulse duration of approximately 20 ps. The experiments were performed using an excitation wavelength at 450 nm. The laser beam was guided through the XY moving stage via three reflecting protected flat aluminum mirrors and focused into the ESI plume via a protected concave reflecting aluminum mirror (f = 100 mm) so that the focal points of the pulsed laser beam and the continuous wavelength laser beam matched. The light emitted was collected in the same way as for steady state experiments. In this case, the optical fiber was connected to a PMT (R1463, Hamamatsu). The fluorescence decay signal was preamplified by a fast preamplifier (350MHz Preamplifier SR445A, Stanford Research) and recorded as a function of time with a fast digital oscilloscope (Lecroy LT322) trigged by a high-speed photodetector (DET10A/M, Thorlabs). 400 sweeps were averaged. Typical fluorescence decays signal are given in Fig. S3 in the supporting information for several points of the ESI plume axis.

Fluorescence decay signals of Tris(2,2′-bipyridyl)dichlororuthenium(II) hexahydrate solutions in methanol and in water were recorded at different temperatures using the home-made temperature-controlled cell in a 90° configuration. Calibration curves were then established in solution giving the fluorescence lifetime of $[Ru(bpy)_3]^{2+}$ as a function of the temperature in methanol (Fig. S4 in supporting information). The fluorescence lifetime was determined by an exponential model using nonlinear least square analysis. The calibration curves obtained were in good agreement with reported temperature-dependent lifetime measurements.[24]

Mie Scattering Setup. An Oxxius Slim 532-300 laser (Oxxius Inc., Santa Clara, CA, USA) was used for excitation. The output power of the laser was 300 mW at 532 nm and its beam diameter 1.05 mm (divergence 1.2 mrad). The laser was injected through the objective using two reflecting protected aluminum flat mirrors (R>90%). The laser at 473 nm was also used for excitation. A system of two cylindrical lenses was used to direct the diffracted light on the Charge Coupled Device (CCD) camera guppy F-080B/C FireWire (Allied Vision Technologies, Stadtroda, Germany). The first lens (f = 100 mm) collected the scattered light for a solid angle ranging from $\theta_{min}=6.7°$ to $\theta_{max}=17.7°$ in relation to the laser beam axis, whereas the second one (f = 150 mm) was used to focus the light on the CCD camera. The first tests of Mie scattering measurements were performed using a piezoelectric droplet generator which produces well-defined spherical droplets (MD-K-130, MicroDrop Technologies) with collection angles $\theta_{min}=6.7°$ and $\theta_{max}=24.5°$ (the collection angle was larger with the droplet generator due to the absence of the ESI source block). Images of the interference patterns recorded from the droplet generator and from the ESI plume are shown in Figs. S5 and S6 in supporting information. The exposure time was set to 80 ms (shutter time is 4000 and time base is 20 μs) and 20 images were recorded for each point.

After plotting the signal intensity as a function of the scattering angle, using a homemade software, comparison with the Mie theory[25] allowed us to obtain the droplet size with accuracy due to the high sensitivity of the interference pattern to the size of the droplets (see Figs. S5 and S6 in supporting information).

Spray Profiles and Data acquisition. The Mie scattering setup, the objective, the continuous wavelength laser and the injection setup of the pulsed laser beam were all mounted on a XYZ moving stage allowing spray profiling. The dimension of the XY images was 15 mm x 6 mm with a step of 0.5 mm in both directions. The control of the moving stage via three step-by-step motors (LMS 80, OWIS) and the data acquisition from the Mie scattering setup, the SSF setup and the TRF setup were piloted by a homemade software application written in VISUALC++. During the acquisition of a spray profile, the spray stability was checked via the MS signal stability. The data were then processed by either Origin 7.5 (OriginLab Corporation) or with Python language (IEP version: 3.5 (source), Platform: win32, Python version: 3.4.1, pyzolib version: 0.3.3, Qt version: 4.8.6, PySide version: 1.2.2).

RESULTS AND DISCUSSION

Temperature profiling of the plume - SST vs TRF. In order to precisely determine the temperature along the spray
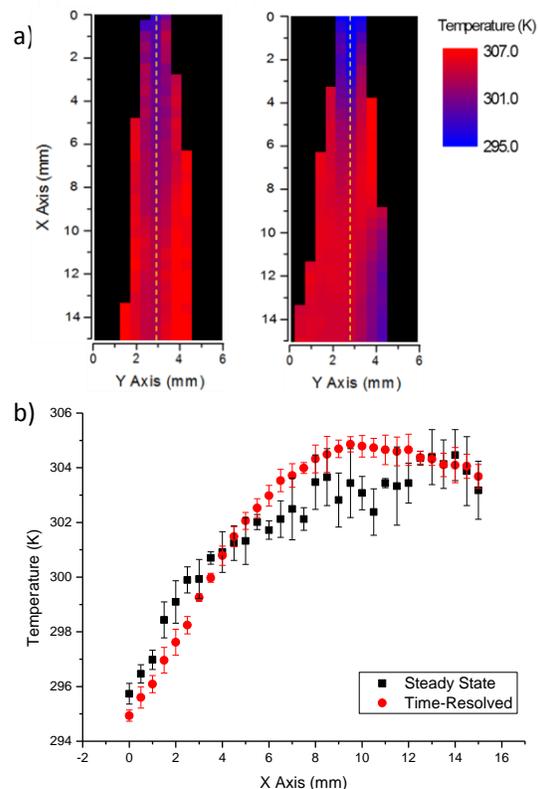
plume, we conducted a comparison between fluorescence lifetime- and intensity-based methods. 2D XY profiles of the temperature of the ESI plume generated in situ by an Agilent Jet Stream Electrospray source are shown in Figure 2. The XY plane is defined by the plane where the intensity of the fluo-

Figure 2: (a) XY profiles of the temperature of the ESI plume from (left) Steady State Fluorescence of a mixture of Rhodamine 110 at 0.2 μM and Rhodamine B at 2 μM in methanol and from (right) Time-Resolved Fluorescence of a solution of $[Ru(bpy)_3]^{2+}$ at 0.1 mM in methanol (SGT = 423 K, SGF = 3 L/min). (b) Axial temperature profiles through the center of the spray from Steady State Fluorescence and from Time-Resolved Fluorescence.

rescence collected was maximal (along the Z axis).

SSF and TRF measurements were performed under the same spray conditions. For SSF, dispersed fluorescence spectra were recorded from a sprayed mixture of Rhodamine 110 at 0.2 μM and Rhodamine B at 2 μM in methanol. The temperature was determined by ratiometry of the intensity at the maximum fluorescence peaks of Rhodamine B band and Rhodamine 110 band (respectively λ_{max}^{RhB} = 567 nm and λ_{max}^{Rh110} = 523 nm) using the calibration curves obtained in solution (see Fig. S1 in supporting information). The exposure time for each step was set to 10 s, the image comprises 403 points and the total acquisition time for a profile is approximatively 4030 s. For TRF, fluorescence decay curves were recorded from a sprayed solution of $[Ru(bpy)_3]^{2+}$ at 0.1 mM in methanol. A typical MS spectrum of a sprayed solution of $[Ru(bpy)_3]^{2+}$ is given in Fig. S7 in supporting information. The temperature was determined by using the fluorescence lifetime calibration curves in solution (see Fig. S4 in supporting information). We recorded decay curves of Ru complex dye at C=10^{-4} M, $5 \cdot 10^{-5}$ M and 10^{-5} M, and we did not observe any change in the life-

times (see Fig. S8 in supporting information). Note that the dye content along the ESI plume decreased by a factor ~2 to ~3. For each step, 400 sweeps were averaged (time for processing the data ~ 5 s), the image comprised 403 points and the total acquisition time for a profile was approximatively 2015 s.

The results clearly indicate that both methods give similar profiles, which excludes potential artifacts causing major analysis errors. The axial temperature profiles through the center of the spray are very similar within the error bars, as shown in bottom of Fig. 2. The different temperatures recorded at X=0 between SSF and TRF can be explained by different initial temperatures in the room for the profiling experiments. Nevertheless, the error bars defined by standard deviations for the four successive replicates of identical acquisitions shows that the TRF method gives more precise results, leading to better visualization of the temperature profile (see fig. 2). For the time resolved fluorescence method, the accuracy (or the error on the measurement) is evaluated to ±0.4 K. The intensity method, shows an initial error measurement of ±0.4K, which gradually increases along the plume to reach ~ ±1.2 K at the bottom of the ESI plume. The decrease in precision for the SSF method is attributed to the decrease in the signal-to-noise ratio of emission spectra due to a lower concentration of dyes at the end of the spray plume. The dependence of dye concentration on the error measurement is lower for the TRF method. Furthermore, the sensitivity of the TRF method, given by the slope of the calibration curve, is -3.71 %K^{-1} in methanol, much higher than that obtained for the SSF method (-0.88 %K^{-1} in methanol), as shown in Figs. S1 and S4 in supporting information.

Under typical electrospray conditions it is estimated that the experimental temperature of the ESI plume varies from 295 K to 307 K. The temperature profile of the ESI plume shows heating of the plume in spite of endothermic solvent evaporation. A lateral gradient temperature is also evident for a small X (top of the ESI plume) and significant recooling can also be highlighted for a larger X and Y (bottom right of the plume). Indeed, two phenomena appear to compete with each other: the evaporation of micrometric droplets leading to the droplet cooling and the conductive thermal transfer between the surrounding gases (super-heated sheath gas) and the solvent, leading to the warming of the droplets. The global warming of the ESI plume indicates that the conductive thermal transfer is predominant (vide infra).

As expected, the temperature is higher at the edges of the electrospray plume where the solvent is in direct contact with the super-heated sheath gas. The recooling at the bottom of the plume can be explained by the presence of the counter-electrode: the position of the capillary inlet of the mass spectrometer is located at X = 15 mm and Y ≃ 8 mm (not shown in the images). The capillary inlet disturbs the flow of heated sheath gas and the endothermic process becomes predominant in this confined zone. Note however that fluorescent species in the gas phase can have significantly longer fluorescence lifetimes than in solution (due to a decrease in the radiative decay rate)[26], which could be problematic for interpretation of the TRF data. We performed additional time-resolved fluorescence measurements with a "non-thermochromic" fluorescent molecule, i.e. Rhodamine 110. The lifetime is almost constant along the spray plume as shown in Fig. S9 in supporting in-

formation. This confirms that the dyes are still solvated even downstream the ESI plume.

TRF Temperature profiling of the plume – Sheath Gas Temperature effect. 2D XY profiles of the ESI plume temperature for three different temperatures of sheath gas are shown in Figure 3. Agilent Jet Stream ESI source design involves using a high temperature for optimal functioning. A predictable effect of the increase in sheath gas temperature can be observed in the XY profiles (see fig. 3a). In particular, the global temperature at the edge of the ESI plume is higher when the sheath gas temperature is higher: from 291 K to 302 K for a sheath gas temperature set at 373 K, from293 K to 303 K for 423 K, and from 298 K to 308 K for 523 K (see fig. 3b). Moreover, the lateral profiles highlight the fact that the edges of the plume electrospray are much more sensitive to surrounding changes in temperature than the core of the plume (se fig. 3c).
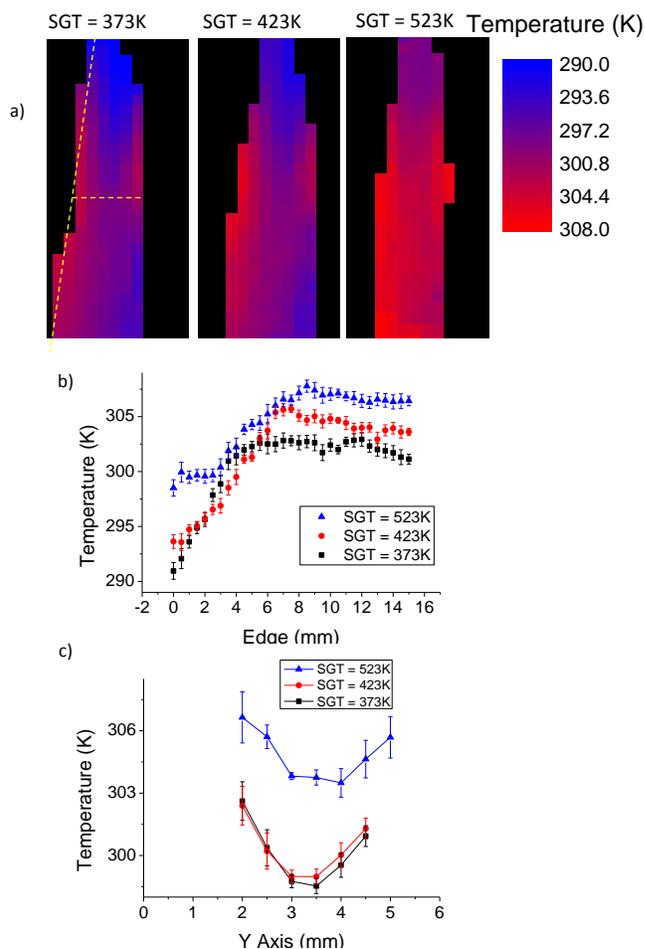

Figure 3: (a) XY profiles from Time-Resolved Fluorescence of a solution of [Ru(bpy)$_3$]$^{2+}$ at 0.1 mM in methanol (SGF = 7 L/min, SGF = 7 L/min) for three different sheath gas temperatures. (b) Axial temperature profiles at the edge of the spray and (c) lateral temperature profile at X = 7.5 mm.

TRF Temperature profiling of the plume – Sheath gas flow rate and nebulizer gas pressure effects. We investigated the impact on spray profiles of other ESI source parameters, i.e. sheath gas flow rate and nebulizer gas pressure. 2D

XY profiles of the ESI plume temperature for different sheath gas flow rates are shown in Figure S10 in supporting information. A homogeneous warming is observed only for the lowest flow rate. The slope of the temperature projection at the edge also shows a significant difference as a function of the flow rate. A steeper slope is observed for lower flow rates. This may be explained by shorter times for thermal equilibration within the plume at lower flow rates. Figure 4 shows the 2D XY images of the ESI plume temperature obtained for different pressures of nebulizer gas (NGP). The Agilent Jet Stream thermal gradient focusing technology was developed to significantly enhance sensitivity in ESI-MS by improving the desolvation and spatial focusing of ions. As shown in Figure 4, the ESI profile changes in dimension and in temperature with the different nebulizer gas pressures. The ESI plume is thinner as the NGP increases because of the spray confinement. Also, the global temperature, both lateral and at the edge of the ESI plume is higher when the nebulizer gas pressure is higher. The ESI profile has been correlated with the MS signal of ions recorded during the image acquisition. The ESI signal is very stable during the acquisition and the standard deviation of the total ion current is only 0.5%. The MS signal of ions increases from 4.5 10^6 counts to 5.5 10^6 counts, with NGP varying from 10 PSI to 50 PSI. This is due to the better desolvation and spatial focusing of ions toward the MS transfer capillary.
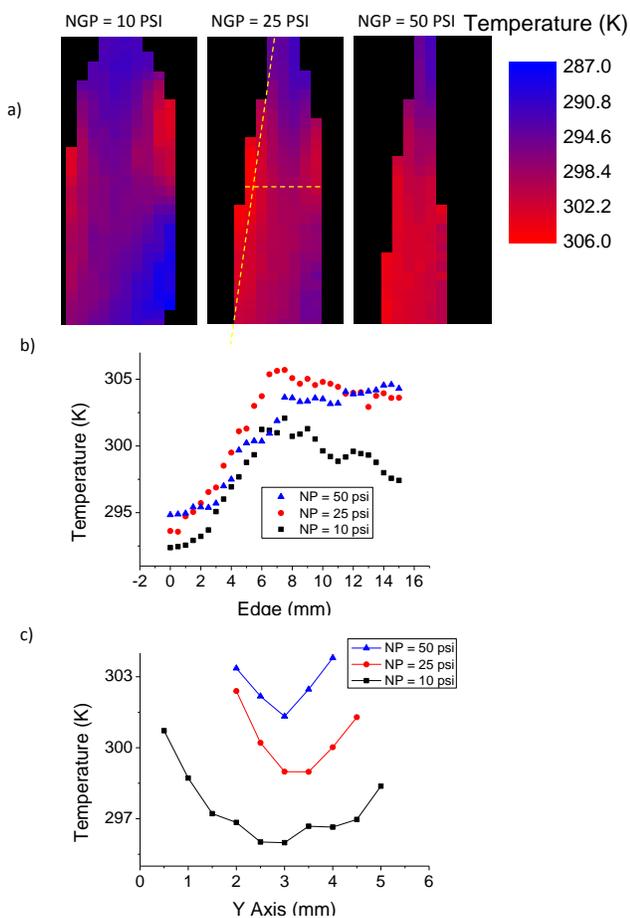
Correlation between temperature and droplet size. For a methanol solution, droplet size along the edge of the ESI plume was measured with the Mie scattering Setup described above. The results show that the size of the droplets along the plume decreases from 4.25 µm to 1.50 µm due to solvent evaporation (See Fig. S11 in supporting information). These values are consistent with previous reported values and confirm efficient desolvation of the electrospray plume as it travels downstream.

The correlation between the experimental temperatures obtained by TRF method and droplet size along the edge of the ESI plume is given in Figure 5. Different models exist for modeling the temperature of evaporating droplets from an ESI plume. The Diffusion Controlled Evaporation Model (DCEM) was adapted by Cook and coworkers[10] for application to electrosprays. This model was first developed by Davies for the airborne droplet evaporation model[27] (see supporting information for more details about the model and the parameters used in this work). Briefly, under proper conditions described by Cook, the temperature evolution results from the competition between the endothermic evaporation of micrometric droplets and the conductive thermal transfer between the surrounding gases (super-heated sheath gas) and the solvent. This can be written as:

$$dT_a = \frac{|Heat\ transfer\ from\ conduction| - |Heat\ transfer\ from\ evaporation|}{m c_{m'}} \quad (1)$$

where dT_a is the change in the temperature of a droplet's surface over an incremental axial distance, m the mass of the droplet and c_m' the specific heat of the solvent in the liquid phase. Considering the geometry of the system, we can express dT_a as:

$$dT_a = \frac{3}{a^2 \rho' c_{m'}} \frac{\delta X}{v} \left\{ k(T_\infty - T_a) - l'D \frac{M}{R_m} \left(\frac{P_a}{T_a} - \frac{P_\infty}{T_\infty} \right) \right\} \quad (2)$$

where a is the radius of the droplet at a given position X, ρ' the volumetric mass density of the solvent in the liquid phase, δX the incremental axial distance, v the velocity of the droplet travelling downstream and considered as a constant parameter ($v = 2$ m/s)[28], k the thermal conductivity of the surrounding medium, T_∞ the temperature of the surrounding medium, l' the latent heat of vaporization of the solvent, D the diffusion coefficient of the solvent vapor in the surrounding medium, M the molar mass, R_m the gas constant, P_a the solvent partial pressure near the surface of the droplet and P_∞ the solvent partial pressure in the surrounding medium.

A simulation of T_a along the edge of the ESI plume can be performed by fitting the experimental value of the droplet radius a along the plume, setting T_∞ as the temperature of the super-heated gas, P_∞ as a fitting parameter and by taking $T_a(X=0)$ as equal to the experimental value recorded for X=0.0 mm. The other parameters, k, l', D and P_a, are temperature dependent and are evaluated respectively by its extrapolated geometrical mean value, its temperature dependence expressions, its geometrical mean value and by the Antoine equation.[29] Simulated droplet temperature as a function of the droplet size is shown in red in Figure 5.

These results show that, in spite of the shrinkage of the droplet due to efficient evaporation, the temperature of the

Figure 4: (a) XY profiles from Time-Resolved Fluorescence of a solution of [Ru(bpy)₃]²⁺ at 0.1 mM in methanol (SGF = 7 L/min and SGT =523 K, SGF = 7 L/min) for three different nebulizer gas pressures. (b) Axial temperature profiles at the edge of the spray and (c) lateral temperature profile at X = 7.5 mm.

system increases due to the super-heated sheath gas effect. Note that this result contrasts with the measurements reported by Cook and coworkers.[10] Indeed, in the work reported by them, droplet temperatures decrease by ~30 K over the first 5.0 mm along the spray axis. However, our set-up is different from that of Cook, in particular concerning the temperature, surrounding gas, and geometry of the ESI source. This impacts on the values of T_∞ and P_∞, which influence the balance between the conduction and evaporation terms in Eqs. 1 and 2.

Experimental data are compared to the optimized diffusion-controlled model at 423 K and 523 K. The model reproduces the measurements qualitatively along the plume for the two different temperatures of the super-heated gas (i.e. 423 K and 523 K). As already mentioned by Cook and coworkers, for the fitting procedure, P_∞ was observed to be the sole fitting parameter affecting final droplet temperature (i.e. plateau observed at ~304 K and ~307 K). Fitted P_∞ values are reasonable and close to the partial pressure of methanol vapor in the surrounding environment at 423 K and 523 K (see Table S1 in supporting information). Thus, in such thermal gradient-focusing electrospray sources, the extent of temperature increase can be modulated by the temperature of the super-heated gas.
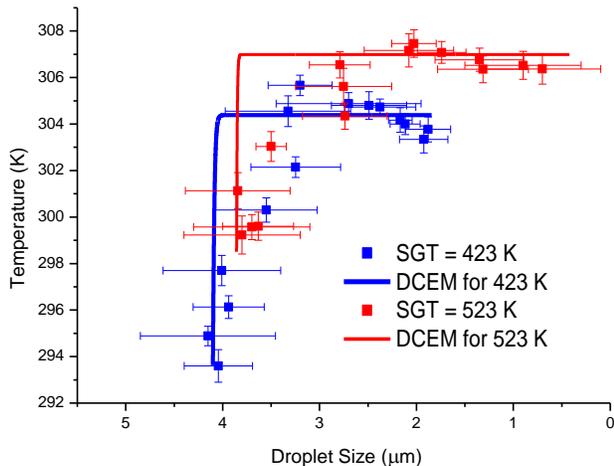

Figure 5 : Correlation between the Temperature and the Droplet size along an edge of the ESI plume for methanol (SGT = 423 K, SGF = 7L/min and SGT = 523 K, SGF = 7L/min). Comparison of experimental data and the optimized diffusion-controlled model at 423 K and 523 K. Error bars for the temperature are given from standard deviations for four successive replicates of the same acquisition and error bars for droplet size are given from the size dispersion of exploitable images collected by the Mie Scattering setup.

The sampling flow rate (F) influences the droplet size. We increased the sampling flow rate in order to be closer to typical flow rate for the LC separation. The maximum rate that we can use in direct infusion mode is 0.2 ml/min (for higher rate, the spray is no more stable). As expected, an increase of droplet size occurs as the flow rate is increased. Initial droplet size is 4.1 μm with F=0.05 mL/min and is 6.5 μm with F=0.2 mL/min (see Fig. S12 in supporting information), in quantitative agreement with the expected dependence in $F^{1/3}$ of the size of the droplets.[30] We managed to follow the correlation between temperature and droplet size within the first 6 mm

along the edge of the spray plume. Downstream, signal due to sub-micron droplets is screened by the light scattering of large droplets (droplets with diameters ranging between 10 and 25 μm are observed in combination to droplet shrinkage). The temperature of the system increases while the size of the droplets decreases for both sampling flow rates, with similar slopes.

CONCLUSION

We profiled the temperature and the size of the droplets as they evaporated in an Agilent Jet Stream electrospray source by measuring both the emission spectra of thermochromics fluorescent dyes and the angular scattering pattern. As temperature indicators, rhodamine dyes were employed for ratiometric intensity based fluorescence techniques. This method was compared to lifetime-based techniques using $[Ru(bpy)_3]^{2+}$. Both methods gave similar profiles; nevertheless, precision and sensitivity were higher for lifetime-based techniques in comparison to intensity-based techniques. This sensitivity makes the $[Ru(bpy)_3]^{2+}$ system particularly suitable for analytical applications.

Global warming of the ESI plume was reported while the size of the droplets decreased along the plume. The global warming (with ΔT ~10 K) indicated that the intake of energy due to the conductive thermal transfer (between the super-heated sheath gas and the solvent) was predominant and stronger than the cooling due to evaporation of droplets. The amplitude of ΔT could be tuned by changing the temperature of the super-heated sheath gas. Thermal gradient focusing ESI sources therefore appear to be efficient sources for evaporating large amounts of solvent and increasing temperature. This change of temperature change may impact on certain chemical equilibria if the kinetics is fast enough to cause changes on the time scale of droplet shrinkage. The amplitude of ΔT may also have consequences on native-MS, as a partial unfolding of proteins may occur during the desolvation process. Fluorescence strategies such as Fluorescence Resonance Energy Transfer (FRET) and time resolved fluorescence could be used to probe the evolution of protein structures along the electrospray plume, in combination with droplet temperature measurements. Measurements with visible dyes tagged to proteins could be implemented easily in our current experimental set-up to better address conformational changes in electrosprayed proteins. Work along these lines is currently underway in our laboratory.

Supporting Information

Deoxygenation protocol for $[Ru(bpy)_3]^{2+}$ solution. Calibration curves for rhodamine and $[Ru(bpy)_3]^{2+}$ dyes in solution and typical fluorescence spectra within the ESI plume. Images of the interference patterns recorded from the droplet generator and from the ESI plume. ESI-MS spectrum of $[Ru(bpy)_3]^{2+}$ in MeOH. Typical Fluorescence decay of a solution of $[Ru(bpy)_3]^{2+}$ in methanol for three different concentration of dye. Fluorescence lifetime of rhodamine 110 in methanol recorded along the center of the spray. XY profiles for three different sheath gas flow rates. The size of a droplet along the plume. Correlation between the temperature and the droplet size along an edge of the ESI plume for two different sampling

flow rates.   Details on modeling: Diffusion Controlled Evaporation.

AUTHOR INFORMATION

Corresponding Author

*Rodolphe Antoine : Address: Institut lumière matière, UMR5306 Université Claude Bernard Lyon1-CNRS, 5 rue de la doua, 69100 Villeurbanne, France. Mail : rodolphe.antoine@univ-lyon1.fr

REFERENCES

(1)   Wong, S. F.; Meng, C. K.; Fenn, J. B. *J. Phys. Chem.* **1988**, *92*, 546-550.

(2)   Fenn, J. B.; Mann, M.; Meng, C. K.; Wong, S. F.; Whitehouse, C. M. *Science* **1989**, *246*, 64.

(3)   Bruins, A.; Cole, R. B., Ed.; John Wiley and Sons, Inc.: Hoboken, N.J. , 2010, pp 123.

(4)   Anacleto, J. F.; Pleasance, S.; Boyd, R. K. *Org. Mass Spectrom.* **1992**, *27*, 660-666.

(5)   Wang, H.; Agnes, G. R. *Anal. Chem.* **1999**, *71*, 4166-4172.

(6)   Wortmann, A.; Kistler-Momotova, A.; Zenobi, R.; Heine, M. C.; Wilhelm, O.; Pratsinis, S. E. *J. Am. Soc. Mass Spectrom.* **2007**, *18*, 385-393.

(7)   Grandori, R.; Matecko, I.; Müller, N. *J. Mass Spectrom.* **2002**, *37*, 191-196.

(8)   Mirza, U. A.; Cohen, S. L.; Chait, B. T. *Anal. Chem.* **1993**, *65*, 1-6.

(9)   Kebarle, P.; Verkerk, U. H. *Mass Spectrom. Rev.* **2009**, *28*, 898-917.

(10)   Gibson, S. C.; Feigerle, C. S.; Cook, K. D. *Anal. Chem.* **2013**, *86*, 464-472.

(11)   Lemoine, F.; Castanet, G. *Exp. Fluids* **2013**, *54*, 1-34.

(12)   Hopkins, R. J.; Reid, J. P. *J. Phys. Chem. A* **2005**, *109*, 7923-7931.

(13)   Zhou, S.; Cook, K. D. *Anal. Chem.* **2000**, *72*, 963.

(14)   Zhou, S.; Edwards, A. G.; Cook, K. D.; Van Berkel, G. J. *Anal. Chem.* **1999**, *71*, 769.

(15)   Zhou, S.; Prebyl, B. S.; Cook, K. D. *Anal. Chem.* **2002**, *74*, 4885.

(16)   Wang, R.; Zenobi, R. *J. Am. Soc. Mass Spectrom.* **2010**, *21*, 378.

(17)   Girod, M.; Dagany, X.; Antoine, R.; Dugourd, P. *Int. J. Mass Spectrom.* **2011**, *308*   41-48.

(18)   Girod, M.; Dagany, X.; Boutou, V.; Broyer, M.; Antoine, R.; Dugourd, P.; Mordehai, A.; Love, C.; Werlich, M.; Fjeldsted, J.; Stafford, G. *Phys. Chem. Chem. Phys.* **2012**, *14*, 9389-9396

(19)   Girod, M.; Antoine, R.; Dugourd, P.; Love, C.; Mordehai, A.; Stafford, G. *J. Am. Soc. Mass Spectrom.* **2012**, *23*, 1221-1231.

(20)   Brites, C. D. S.; Lima, P. P.; Silva, N. J. O.; Millan, A.; Amaral, V. S.; Palacio, F.; Carlos, L. D. *Nanoscale* **2012**, *4*, 4799-4829.

(21)   Jaque, D.; Vetrone, F. *Nanoscale* **2012**, *4*, 4301-4326.

(22)   Paviolo, C.; Clayton, A. H. A.; McArthur, S. L.; Stoddart, P. R. *J. Microsc.* **2013**, *250*, 179-188.

(23)   Mordehai, A. In *Proceedings of the 57th ASMS Conference on Mass Spectrometry & Allied Topics*: Philadelphia, Pennsylvania, 2009.

(24)   Brennaman, M. K.; Meyer, T. J.; Papanikolas, J. M. *J. Phys. Chem. A* **2004**, *108*, 9938-9944.

(25)   Bohren, C. F.; Huffman, D. R. *Absorption and scattering of light by small particles*; Wiley, 1998.

(26)   Frankevich, V.; Chagovets, V.; Widjaja, F.; Barylyuk, K.; Yang, Z.; Zenobi, R. *Phys. Chem. Chem. Phys.* **2014**, *16*, 8911-8920.

(27)   Davies, C. N.; Shaw, D. T., Ed.; Wiley-Interscience: New York, 1978.

(28)   Nemes, P.; Marginean, I.; Vertes, A. *Anal. Chem.* **2007**, *79*, 3105.

(29)   NIST Chemistry Web Book. Available at http://webbook.nist.gov/chemistry/. Accessed 18 September.

(30)   Fernandez de la Mora, J.; Loscertales, I. G. *J. Fluid Mech.* **1994**, *260*, 155-184.

Graphical TOC